Electronic band structure and exchange coupling constants in ACr_2X_4 spinels (A=Zn, Cd, Hg; X=O, S, Se)

A. N. Yaresko
Max Planck Institute for the Physics of Complex Systems, D-01187 Dresden, Germany
(Received 12 October 2007; revised manuscript received 1 February 2008; published 5 March 2008)

We present the results of band structure calculations for ACr_2X_4 (A=Zn, Cd, Hg and X=O, S, Se) spinels. Effective exchange coupling constants between Cr spins are determined by fitting the energy of spin spirals to a classical Heisenberg model. The calculations reproduce the change of the sign of the dominant nearest-neighbor exchange interaction J_1 from antiferromagnetic in oxides to ferromagnetic in sulfides and selenides. It is verified that the ferromagnetic contribution to J_1 is due to indirect hopping between Cr t_{2g} and e_g states via X p states. Antiferromagnetic coupling between third Cr neighbors is found to be important in all the ACr_2X_4 spinels studied, whereas other interactions are much weaker. The results are compared to predictions based on the Goodenough–Kanamori rules of superexchange.

DOI: 10.1103/PhysRevB.77.115106 PACS number(s): 71.20.−b, 71.70.Gm, 75.30.Et

I. INTRODUCTION

Chromium spinels provide unrivalled possibilities for studying magnetic interactions in solids. In these compounds with a general formula ACr_2X_4, where A is a divalent nonmagnetic cation (Mg, Zn, Cd, or Hg) and X is a divalent anion (O, S, or Se), a Cr^{3+} ion is in the $3d^3$ configuration. Its three $3d$ electrons occupy the majority-spin states of a completely spin polarized t_{2g} subshell leading to the total spin $S=3/2$. Although charge and orbital degrees of freedom in the ACr_2X_4 spinels are frozen, these compounds show wide variety of magnetic properties ranging from those of a strongly frustrated antiferromagnet to a Heisenberg ferromagnet. Depending on the chemical composition their effective Curie–Weiss temperature (Θ_{CW}) varies from −400 K in oxides to 200 K in selenides,[1,2] which indicates that the sign of the dominant exchange interaction changes from antiferromagnetic (AFM) to a ferromagnetic (FM) one.

In the ACr_2O_4 spinels, AFM nearest-neighbor interactions between Cr spins residing on a pyrochlore lattice are geometrically frustrated. The magnetic ground state of a frustrated antiferromagnet is highly degenerate which leads to unusual low-temperature properties.[3,4] Cr oxide spinels remain paramagnetic with the Curie–Weiss form of the magnetic susceptibility down to temperatures well below $|\Theta_{CW}|$ of 398, 71, and 32 K for A=Zn, Cd, and Hg. $ZnCr_2O_4$ (T_N =12.5 K) and $CdCr_2O_4$ (T_N=7.8 K) undergo a first order phase transition of the Spin–Peierls type into a magnetically ordered Néel state at temperatures much lower than the characteristic strength $|\Theta_{CW}|$ of the interaction between Cr spins.[5,6] The transitions are accompanied by cubic to tetragonal structural distortions; however, the sign of the distortions and the magnetic order below T_N are different. In $ZnCr_2O_4$, the lattice contracts along the c axis ($c<a$) and the Néel state has a complex commensurate spin structure with four characteristic wave vectors. In contrast, the lattice of $CdCr_2O_4$ expands below T_N ($c>a$) and its ordered state is incommensurate with a wave vector $\mathbf{Q}=(0,\delta,1)$ with $\delta \sim 0.09$.[7] $HgCr_2O_4$ also undergoes a transition to a magnetically ordered state at T_N=5.8 K but the symmetry of the lattice lowers to orthorhombic.[8] Recently, a metamagnetic transition and a wide magnetization plateau with the magnetic moment equal to one-half of the full Cr moment have been observed in $CdCr_2O_4$ and $HgCr_2O_4$.[6,8–10]

In $ACr_2S(e)_4$ spinels, dominant ferromagnetic interactions are not geometrically frustrated. Nevertheless, Cr spins in $ZnCr_2S_4$ and $ZnCr_2Se_4$ form helical spin structures below 15.5 and 18 K, respectively.[11–13] In $ZnCr_2S_4$, the helical structure coexists at low temperatures with a collinear AFM one. The transitions into helically ordered state are supposed to occur because of competing FM nearest-neighbor interaction and AFM interactions between more distant Cr neighbors. Recently, it has been shown that $CdCr_2S_4$ and $HgCr_2S_4$ exhibit ferroelectric behavior with strong increase of the dielectric constant below the temperature of magnetic ordering.[14,15]

The diversity of magnetic properties of the ACr_2X_4 spinels can hardly be explained without understanding the mechanism of exchange interactions between Cr spins, their range, and relative strengths. So far, theoretical analyses of the effective exchange interactions in Cr spinels were mostly based on the Goodenough–Kanamori rules of superexchange.[16,17] Goodenough in Ref. 18 explained the FM sign of the nearest-neighbor coupling J_1 in $ACr_2S(e)_4$ by indirect hopping between half-filled Cr t_{2g} and empty e_g states via p states of X anions. Dwight and Menyuk[19,20] analyzed various superexchange paths for interactions between up to sixth Cr neighbors and concluded that AFM coupling constants J_3 between third neighbors and even weaker FM J_4 and J_6 may be relevant alongside J_1. Then, the estimated J_n were used to examine the stability of different spiral ground states in $ZnCr_2Se_4$. To our knowledge, the only attempt to obtain the values of J_n from *ab initio* band structure calculations was made in Ref. 21 where the coupling constants J_1-J_3 were calculated by comparing the total energies of several simple spin configurations.

The aim of the present work is to compare electronic band structures of ACr_2X_4 (A=Zn, Cd, Hg and X=O, S, Se) spinels calculated within the local spin-density approximation (LSDA) and LSDA+U and to estimate exchange coupling constants between Cr spins by fitting the calculated energy of spin spirals to a classical Heisenberg model. The

TABLE I. Experimental lattice constants a_0 (Å) and fractional coordinate x of X ions used in the calculations and the shortest Cr-Cr, Cr-X, and A-X distances (Å). The last column contains experimental values of Θ_{CW} taken from Ref. 2.

Compound	a	x	$d_{Cr\text{-}Cr}$	$d_{Cr\text{-}X}$	$d_{A\text{-}X}$	Θ_{CW}
$ZnCr_2O_4$[a]	8.327	0.2616	2.944	1.990	1.970	−398
$CdCr_2O_4$[b]	8.600	0.2682	3.041	2.006	2.133	−71
$HgCr_2O_4$[b]	8.661	0.2706	3.062	2.003	2.184	−32
$ZnCr_2S_4$[c]	9.982	0.2619	3.529	2.383	2.367	7.9
$CdCr_2S_4$[d]	10.240	0.2647	3.620	2.419	2.478	90
$HgCr_2S_4$[e]	10.256	0.267	3.626	2.402	2.523	140
$ZnCr_2Se_4$[f]	10.484	0.2599	3.707	2.522	2.450	155
$CdCr_2Se_4$[g]	10.735	0.2642	3.795	2.540	2.588	184
$HgCr_2Se_4$[e]	10.737	0.264	3.796	2.543	2.585	200

[a]Reference 22.
[b]Reference 10.
[c]Reference 23.
[d]Reference 24.
[e]Reference 2.
[f]Reference 11.
[g]Reference 25.

paper is organized as follows. The spinel crystal structure is shortly described in Sec. II. Some details of the calculational procedure are given in Sec. III. In Sec. IV, the band structures of the ACr_2X_4 spinels calculated using LSDA and LSDA+U are compared and their dependence on the chemical composition is analyzed. The results on the exchange coupling constants J_n are presented in Sec. V. The comparison of calculated J_n to experimental data and the discussion of their origins are given in Sec. VI. Finally, the results are summarized in Sec. VII.

II. CRYSTAL STRUCTURE

ACr_2X_4 compounds considered here belong to a large family of $A^{2+}B_2^{3+}X_4^{2-}$ spinels which crystallize to a cubic $Fd\bar{3}m$ (N227) structure, with A, B, and X ions occupying 8a (1/8,1/8,1/8), 16d (1/2,1/2,1/2), and 32e (x,x,x) Wyckoff positions, respectively. The experimental values of the lattice constant (a_0) and fractional coordinates (x) are collected in Table I. The spinel crystal structure plotted in Fig. 1 can be considered as built of distorted Cr_4X_4 cubes which share a Cr site. Cr and X ions that belong to the same cube form two regular tetrahedra with a common center, which coincides with the center of the cube. Each cube is linked via X ions to four regular AX_4 tetrahedra. The centers of the Cr_4X_4 cubes and AX_4 tetrahedra form two diamond lattices shifted by a vector (1/4,1/4,1/4). Finally, Cr ions are arranged along chains running in the ⟨110⟩ directions and form the so-called pyrochlore lattice which consists of corner-sharing regular tetrahedra.

As the ionic radius of a A^{2+} cation increases in the row $Zn^{2+}\rightarrow Cd^{2+}\rightarrow Hg^{2+}$, X ions are pushed further away from the center of a AX_4 tetrahedron. This leads to lattice expansion and corresponding increase of Cr-Cr distances. The distortion of Cr_4X_4 cubes also increases in order to avoid too strong elongation of Cr-X bonds and manifests itself in the increase of the x parameter. When O^{2-} ions are replaced by S^{2-} or Se^{2-}, which have significantly larger ionic radii, the length of both A-X and Cr-X bonds increases. This results in even stronger increase of the lattice constant. The nearest Cr-Cr (d_{Cr-Cr}), Cr-X ($d_{Cr\text{-}X}$), and A-X ($d_{A\text{-}X}$) distances are summarized in Table I.

Each Cr site is surrounded by a trigonally distorted X_6 octahedron, with all Cr-X distances in the octahedron being equal. The degree of the trigonal distortion is determined by the value of the fractional coordinate x. For $x>0.25$, the octahedron is expanded along one of the ⟨111⟩ directions and becomes regular for $x=1/4$.

The local symmetry of a Cr site is D_{3d}. It is worth noting that since six Cr ions nearest to a Cr site form a trigonal antiprism, the symmetry remains trigonal even when x is equal to the ideal value of 1/4.

III. COMPUTATIONAL DETAILS

The calculations of the electronic band structure of the ACr_2X_4 spinels were performed for the experimentally ob-

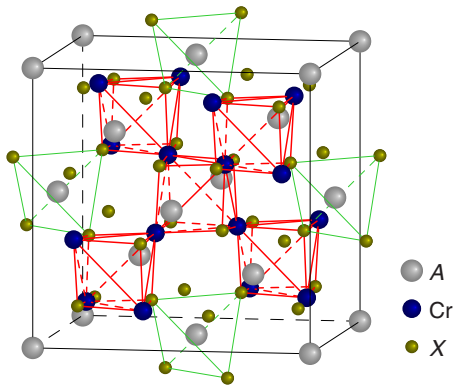

FIG. 1. (Color online) The crystal structure of ACr_2X_4 spinels with an A ion shifted to the origin. Distorted Cr_4X_4 cubes and AX_4 tetrahedra are plotted by thick (red) and thin (green) lines, respectively.

served lattice constant and X fractional coordinates (Table I) on the base of the local spin-density approximation[26] to the density functional theory[27,28] using the linear muffin-tin orbital (LMTO) method[29] with the combined correction terms taken into account. In order to decrease the overlap between atomic spheres, three sets of empty spheres (E) were added at 8b (0,0,0), 16c (3/8,3/8,3/8), and 48f (x',1/8,1/8) Wyckoff positions. Muffin-tin orbitals with angular momentum $l \leqslant 2$ for A, Cr, and X spheres and $l \leqslant 1$ for empty spheres were included into the basis set. The Perdew–Wang parametrization[30] for the LSDA exchange-correlation potential was used. Brillouin zone (BZ) integrations were performed using the improved tetrahedron method.[31]

Calculations for spiral spin structures based on the generalized Bloch theorem[32] were performed under the assumption that the direction of the magnetization $\mathbf{m}$ is constant within each atomic sphere. Inside a sphere at $\mathbf{t}+\mathbf{R}$, where $\mathbf{t}$ defines its position in a unit cell and $\mathbf{R}$ is a lattice vector, the magnetization direction is determined by an angle θ_t between the spin moment and z axis, the wave vector $\mathbf{q}$ of a spiral, and a phase ϕ_t,

$$\mathbf{m}(\mathbf{r}_t) = m(r_t)\begin{pmatrix} \cos(\phi_t + \mathbf{q}\cdot\mathbf{R})\sin\theta_t \\ \sin(\phi_t + \mathbf{q}\cdot\mathbf{R})\sin\theta_t \\ \cos\theta_t \end{pmatrix}, \tag{1}$$

with $\mathbf{r}_t = \mathbf{r} - \mathbf{t} - \mathbf{R}$.

When performing LMTO calculations for spin spirals, it is convenient to split the LSDA exchange-correlation potential into a spin- and $\mathbf{q}$-independent part $V=(V_\uparrow+V_\downarrow)/2$ and an effective exchange field $B=(V_\uparrow-V_\downarrow)/2$, where $V_\uparrow$ and $V_\downarrow$ are exchange-correlation potentials for majority- and minority-spin electrons defined in the site-dependent local spin frame, in which the spin-density matrix for a given site is diagonal. In the present calculations, *spin-independent* LMTO basis functions were constructed starting from the solution of the Kohn–Sham equation with only the spin-independent part V of the exchange-correlation potential included to the LSDA one electron potential. Matrix elements of the spin-dependent part of the LMTO Hamiltonian,

$$H_B = \sum_{\mathbf{t},\mathbf{R}} \mathbf{B}(\mathbf{r}_t)\cdot\boldsymbol{\sigma} = \sum_{\mathbf{t}} B(r_t)\begin{pmatrix} \cos\theta_t & \sin\theta_t \sum_{\mathbf{R}} e^{-i(\phi_t+\mathbf{q}\cdot\mathbf{R})} \\ \sin\theta_t \sum_{\mathbf{R}} e^{i(\phi_t+\mathbf{q}\cdot\mathbf{R})} & -\cos\theta_t \end{pmatrix}, \tag{2}$$

where $\boldsymbol{\sigma}$ is a vector of Pauli matrices, were included at a variational step. Radial matrix elements of $B(r)$ between the solution of the Kohn–Sham equation inside a sphere $\phi_\nu(r)$ and/or its energy derivative $\dot{\phi}_\nu(r)$ were calculated by numerical integration.

The diagonal in spin indices matrix elements of H_B calculated between two Bloch wave functions with wave vectors $\mathbf{k}$ and $\mathbf{k}'$ do not depend on $\mathbf{q}$ and, as usual, are nonzero only if $\mathbf{k}=\mathbf{k}'$. In the absence of the spin-orbit coupling, the only off-diagonal in spin indices terms of the Hamiltonian are $H_B^{\downarrow\uparrow}(\mathbf{q})$ and $H_B^{\uparrow\downarrow}(\mathbf{q})$ given by Eq. (2), which couple the states with $\mathbf{k}'-\mathbf{k}=\pm\mathbf{q}$. Then, the LMTO Hamiltonian matrix can be written in the following block form:

$$H = \begin{pmatrix} H^{\downarrow\downarrow}_{\mathbf{k}-\mathbf{q}/2,\mathbf{k}-\mathbf{q}/2} & H^{\downarrow\uparrow}_{\mathbf{k}-\mathbf{q}/2,\mathbf{k}+\mathbf{q}/2} \\ H^{\uparrow\downarrow}_{\mathbf{k}+\mathbf{q}/2,\mathbf{k}-\mathbf{q}/2} & H^{\uparrow\uparrow}_{\mathbf{k}+\mathbf{q}/2,\mathbf{k}+\mathbf{q}/2} \end{pmatrix}. \tag{3}$$

Thus, for a spin spiral with an arbitrary $\mathbf{q}$ one needs to diagonalize one $2N\times 2N$ matrix instead of two $N\times N$ matrices, one for each spin channel, in conventional spin-polarized calculations.[32] If, however, the spin-orbit coupling term is included into the Hamiltonian, it additionally couples majority- and minority-spin states with the same $\mathbf{k}$ and the Hamiltonian matrix becomes infinite.

Most calculations reported in Sec. V were performed for planar spin spirals with all $\theta_t=\pi/2$. Then, for a given $\mathbf{q}$, the magnetization direction inside a sphere is defined solely by the phase ϕ_t. The phases at Cr sites were fixed by requiring that $\phi_t=\mathbf{q}\cdot\mathbf{t}$. At other atomic and empty sites, they were determined self-consistently. At each iteration of a self-consistency loop, a rotation to the local spin frame in which the spin-density matrix becomes diagonal was found and the corresponding rotation angles were used to determine new magnetization direction for the next iteration.[33] Iterations were repeated until self-consistency in the electron spin density as well as in the magnetization direction in each atomic sphere was achieved.

Finally, in order to account for correlation effects in the Cr 3d shell, we adopted the LSDA+U method[34] in the rotationally invariant representation.[35,36] The so-called atomic limit[37] was used for the double counting term. The effective screened Coulomb repulsion U between 3d electrons was considered as a parameter of the model and varied from 2 to 4 eV. For the on-site exchange integral J_H, the value of 0.9 eV estimated from the LSDA calculations was used.

IV. COMPARISON OF THE ELECTRONIC STRUCTURES OF O-, S-, AND S-BASED SPINELS

A. Spin-restricted local density approximation results and hopping matrix elements

The effect of the chemical composition on the electronic structure of ACr_2X_4 spinels can be analyzed by comparing the densities of Cr d and X p states obtained from spin-restricted LDA calculations for ACr_2X_4 (Fig. 2). Since site-resolved densities of states (DOSs) for the ACr_2S_4 spinels show the same trends as those for ACr_2Se_4, only DOSs calculated for ACr_2O_4 and ACr_2Se_4 compounds are presented in Fig. 2.

In all the ACr_2X_4 spinels considered in the present work, occupied bands in the energy range down to −10 eV below the Fermi level (E_F) originate from A d, Cr d, and X p states. A d states in the sulfides and selenides as well as Cd 4d states in $CdCr_2O_4$ form a narrow group of bands below the bottom of X p states. Zn 3d and Hg 5d bands in the corresponding oxides cross the bottom of O p states and hybridize strongly with the latter which results in the appearance of wide peaks of d DOS between −9 and −7 eV. The A d states are com-

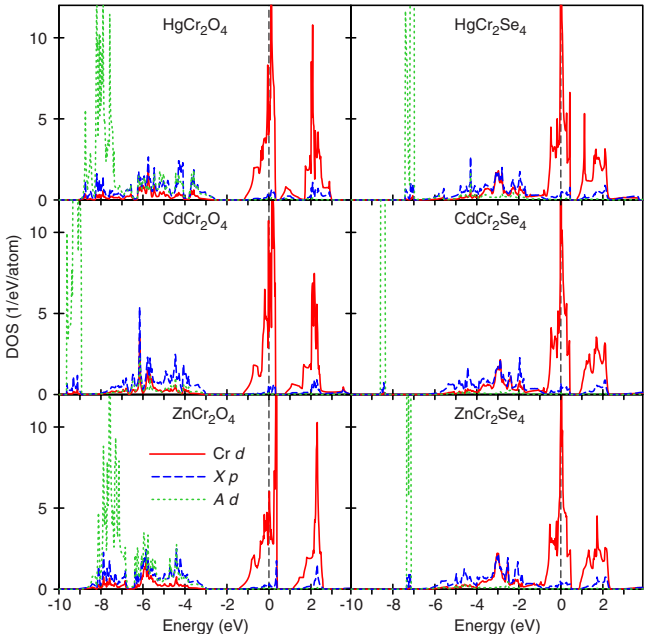

FIG. 2. (Color online) Densities of Cr d (red solid lines), X p (blue dashed lines), and A d (green dotted lines) states in ACr_2O_4 and ACr_2Se_4. Zero energy is chosen at the Fermi level.

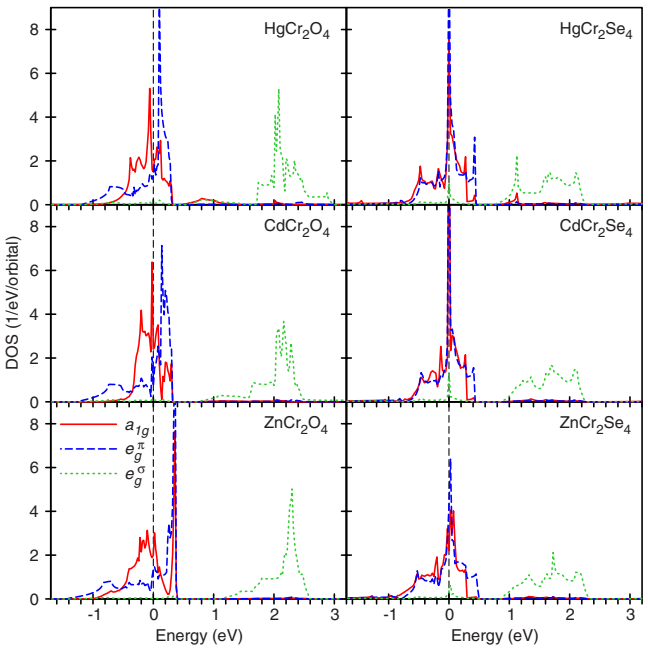

FIG. 3. (Color online) Symmetry-resolved densities of the Cr d a_{1g} (red solid lines), e_g^{π} (blue dashed lines), and e_g^{σ} (green dotted lines) states in ACr_2O_4 and ACr_2Se_4. Zero energy is chosen at the Fermi level.

pletely occupied and lie well below E_F so that they have no effect on the magnetic properties of the ACr_2X_4 spinels.

O p-derived bands in ACr_2O_4 spread over the energy range from -8 to -3 eV and are separated by a gap of $\sim$1.5 eV from Cr $3d$ states which give prevailing contribution to the bands crossing the Fermi level and a prominent DOS peak at E_F. Because of the decrease of the binding energy of valence p states with the increase of the X atomic number S $3p$ and Se $4p$ states in $ACr_2S(e)_4$ spinels move closer to E_F and form bands between -6.5 and -0.5 eV. In contrast to oxides the top of X p bands overlaps with the bottom of Cr d ones and the gap between X p and Cr d states closes.

Cr d states are split by the cubic component of the crystal field at a Cr site into a triplet t_{2g} (d_{xy}, d_{zx}, and d_{yz}) and a doublet e_g (d_{3z^2-1} and $d_{x^2-y^2}$). In a Cr X_6 octahedron, the t_{2g} and e_g states form relatively weak $pd\pi$- and much stronger $pd\sigma$-type bonds with the X p states, respectively. Bonding Cr d-X p combinations participate in the formation of the X p-derived bands which is evidenced by the rather high density of Cr d states in this energy range (see Fig. 2). These states are completely filled and stabilize the Cr X_6 octahedron. In all the ACr_2X_4 spinels considered here, the partially occupied bands crossing E_F are formed by antibonding combinations of the Cr d t_{2g} and X p states with the dominant contribution of the former. These states, filled with three electrons, play the crucial role in the formation of Cr magnetic moments and effective exchange interactions between them. The Cr d states of the e_g symmetry which form antibonding $pd\sigma$ combinations with the X p states are shifted to higher energies and separated by an energy gap from the antibonding Cr t_{2g}-X p states. For the sake of brevity, in the following, these bands are referred to simply as Cr d t_{2g} and e_g bands.

As the local symmetry of a Cr site is lower than cubic the t_{2g} states are additionally split into a singlet and a doublet which transform according to a_{1g} and e_g representations of the D_{3d} group. We denote this doublet as e_g^{π} in order to distinguish it from the doublet formed by d_{3z^2-1} and $d_{x^2-y^2}$ orbitals (e_g^{σ}) which transforms according to the same e_g representation. The densities of the Cr d states of a_{1g}, e_g^{π}, and e_g^{σ} symmetries are shown in Fig. 3.

The trigonal splitting between the a_{1g} and e_g^{π} states is much smaller than their bandwidths, with the center of gravity of the former being about 0.05 eV lower. The corresponding DOS curves in ACr_2O_4 are, however, remarkably different. The total width of the Cr t_{2g} subband is determined by the e_g^{π} states. Their DOS curve is very asymmetric with low DOS at the bottom and a huge DOS peak at the top of the t_{2g} bands. The a_{1g} states are significantly narrower. They are responsible for the DOS peak at E_F but contribute also to the high-energy e_g^{π} DOS peak. This strong suppression of the width of the a_{1g} DOS is a characteristic feature of $3d$ transition metal oxides with the spinel structure and a small ionic radius of an A ion. Recently, two scenarios based on a strong Coulomb interaction within V d shell and the localized behavior of V a_{1g} states have been proposed to explain heavy-fermion-like properties in LiV_2O_4.[38,39]

An analysis using Slater–Koster integrals[40] shows that the narrowing of a_{1g} DOS is caused by the competition of direct d-d hopping matrix elements t_{dd} between the Cr t_{2g} states and an effective indirect hopping t_{dd}^p via O p states. The latter is of the order of $t_{pd}^2/(\varepsilon_d-\varepsilon_p)$, where t_{pd} is a Cr d-O p hopping and ε_p and ε_d are the energies of the Cr d and O p states, and is very sensitive to the deviation of the fractional coordinate x from the ideal value of 1/4, i.e., the degree of the distortion

of CrO_6 octahedra. As it was shown for LiV_2O_4 in Ref. 41 and verified for $ZnCr_2O_4$ in the present work, the densities of a_{1g} and e_g^π states calculated for a hypothetical spinel structure with $x=1/4$ are of the same width, whereas for experimental values of $x\approx 0.26-0.27$, the competition between the direct and indirect contributions to the effective d-d hopping leads to reduction of the a_{1g} bandwidth relative to the width of e_g^π states. Finishing the discussion of the d-d hybridization, we have to mention strong hopping matrix elements between t_{2g} and e_g^σ states which appear as a result of either direct hopping between, for instance, d_{xy} and d_{3z^2-1} orbitals in the [110] direction or indirect one via p_x and p_y states of two X ions closest to the Cr-Cr bond, which is allowed already in an undistorted Cr_4X_4 cube. The direct and indirect contributions are of opposite signs which may lead to strong suppression of effective $t_{2g}-e_g^\sigma$ hopping matrix elements.

Let us come back to the results of band structure calculations shown in Figs. 2 and 3. As Zn is replaced by a larger Cd or Hg ion, the width of the Cr t_{2g} states decreases from 1.8 eV in $ZnCr_2O_4$ to 1.6 eV in $HgCr_2O_4$. The narrowing of the bands can be explained by the reduction of the strength of both d-d and Cr d-O p hopping matrix elements caused by the lattice expansion (see Table I). The shape of a_{1g} and e_g^π DOS, however, also varies considerably. This indicates the change of relative strengths of the direct d-d and indirect d-O p-d hoppings between Cr t_{2g} states.

Cr e_g^σ states are affected much stronger by the change of the chemical composition because of their interaction with s bands of an A ion. In $ZnCr_2O_4$, e_g^σ bands cross just the bottom of a Zn 4s band near the BZ center. Cd 5s and, especially, Hg 6s bands shift to lower energies and overlap with Cr e_g^σ bands. In $CdCr_2O_4$, the hybridization with a Cd 5s band is responsible for a low energy tail of Cr e_g^σ DOS. In $HgCr_2O_4$, the bottom of a Hg 6s band comes so close to Cr t_{2g} bands that it starts to hybridize via O p states with Cr a_{1g} bands, which is evidenced by the appearance of noticeable density of a_{1g} and e_g^σ states in the energy gap between t_{2g}- and e_g^σ-derived bands.

Symmetry-resolved densities of Cr d states in selenides, presented on the right hand side of Fig. 3, are strikingly different from the corresponding DOS curves in oxides. The densities of a_{1g} and e_g^π states do not differ so much as in oxides, with the top of the e_g^π bands being shifted to somewhat higher energies. The huge DOS peak found at the very top of the t_{2g} states in $ZnCr_2O_4$ and slightly lower in the two other oxides shifts in selenides closer to the center of the t_{2g} bands. The energy difference between the Cr e_g^σ and t_{2g} states is somewhat smaller than in oxides. The e_g^σ DOS curves become wider and more symmetric. Another important distinction of the $ACr_2S(e)_4$ electronic structure is the enhanced weight of the e_g^σ states in the Bloch wave functions of Cr t_{2g} bands, which is revealed by noticeable density of the e_g^σ states in the corresponding energy range.

The difference between the dispersions of Cr d bands in the oxides and selenides is illustrated in Fig. 4 which shows "fat" bands calculated for $ZnCr_2O_4$ and $ZnCr_2Se_4$, with the size of filled circles and squares being proportional to the partial weight of Cr a_{1g} and e_g^σ states, respectively, in the Bloch wave function at a given $\mathbf{k}$ point.

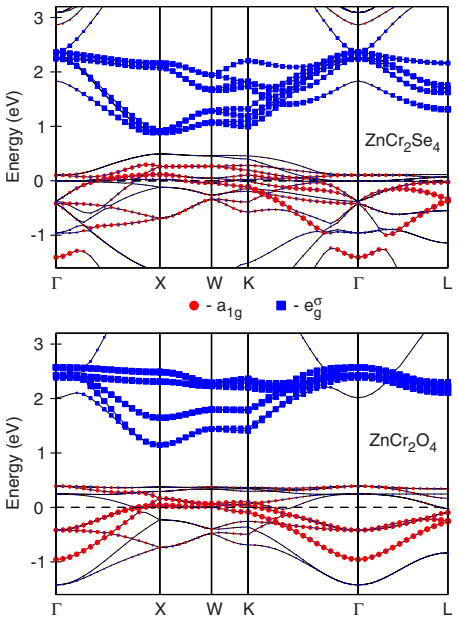

FIG. 4. (Color online) "Fat" bands calculated along some symmetry lines in the fcc BZ for $ZnCr_2O_4$ (lower panel) and $ZnCr_2Se_4$ (upper panel). The size of filled (red) circles and (blue) squares is proportional to the partial weight of Cr a_{1g} and e_g^σ states in the Bloch wave function, respectively. Zero energy is chosen at the Fermi level.

The above-mentioned differences in the band dispersions and DOS suggest that the effective d-d hopping matrix elements should also be significantly different, which is not surprising taking into account the increase of the lattice constants in $ACr_2S(e)_4$ as compared to ACr_2O_4 (Table I). The increase of Cr-Cr distances leads to strong reduction of the direct d-d hopping matrix elements which fall off as $1/d_{\text{Cr-Cr}}^5$. It should be noted, however, that a tight binding analysis of the band structure of $CdCr_2S_4$ performed in Ref. 42 showed that the direct hopping between Cr d states is not negligible even in sulfides and selenides. The contribution of the indirect hopping via X p states to the effective d-d hoppings, which is proportional to $t_{pd}^2/(\varepsilon_d-\varepsilon_p)$, does not change much because (i) S 3p and Se 4p states are significantly more spatially extended than O 2p states and, although $d_{\text{Cr-}X}$ also increases in $ACr_2S(e)_4$, Cr d-X p hoppings t_{pd} remain approximately of the same strength as in ACr_2O_4, and (ii) the energy difference $\varepsilon_d-\varepsilon_p$ in sulfides and selenides is smaller than in oxides.

Similar to oxides the Cr t_{2g} states in selenides become narrower with the increase of the A ionic radius. The hybridization of Cr e_g^σ states with Hg 6s bands leads to sharpening of a DOS peak near the bottom of the e_g^σ subband.

B. Effect of spin polarization

When in spin-polarized LSDA calculations Cr d states with two spin projections are allowed to have different occupations, the strong on-site exchange interaction splits the half-filled Cr t_{2g} shell into occupied majority-spin $t_{2g\uparrow}$ and unoccupied minority-spin $t_{2g\downarrow}$. The densities of Cr d and X p

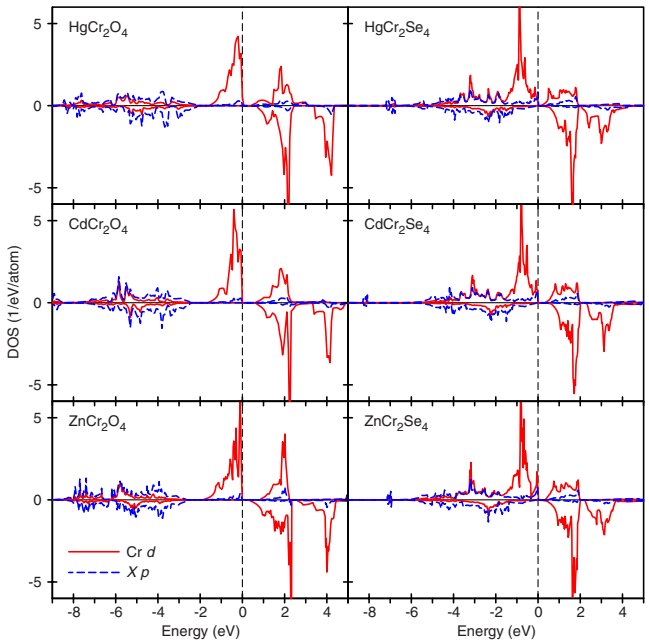

FIG. 5. (Color online) Cr d (red solid lines) and $X\,p$ (blue dashed lines) DOS in ACr_2O_4 and ACr_2Se_4 obtained from spin-polarized calculations with FM alignment of Cr magnetic moments. Zero energy is at the Fermi level.

states in ACr_2O_4 and ACr_2Se_4 obtained from spin-polarized calculations with the FM alignment of Cr moments are shown in Fig. 5. Majority- and minority-spin fat bands calculated for $ZnCr_2O_4$ and $ZnCr_2Se_4$ are presented in Figs. 6 and 7.

In all the spinels studied here, the exchange splitting of Cr d states is about 2.7 eV which gives an estimate of 0.9 eV for the on-site Hund's exchange coupling J_H. The exchange and crystal field splittings are of comparable strengths, so that Cr $t_{2g\downarrow}$ states are found at the same energy as $e^{\sigma}_{g\uparrow}$. In the oxides, $t_{2g\uparrow}$ states remain separated by an energy gap from O p bands. In $ZnCr_2O_4$ and $CdCr_2O_4$, the FM solution is insulating with completely occupied $t_{2g\uparrow}$ and empty $t_{2g\downarrow}$ states. In $HgCr_2O_4$, the bottom of a minority-spin Hg s band hybridized with Cr $a_{1g\downarrow}$ states crosses $t_{2g\uparrow}$ bands leading to a metallic solution.

In contrast to the oxides, in the $ACr_2S(e)_4$ spinels, $t_{2g\uparrow}$ states move below the top of the $X\,p$ states (Fig. 7). As a result, the highest occupied majority-spin bands are formed mainly by $X\,p$ states strongly hybridized with Cr $e^{\pi}_{g\uparrow}$. In the Zn and Hg spinels, they overlap with the very bottom of mostly unoccupied $t_{2g\downarrow}$ bands, while for $CdCr_2S_4$ and $CdCr_2Se_4$, insulating solutions with a tiny gap were obtained. The LSDA band structures and DOS calculated for $CdCr_2S_4$ and $CdCr_2Se_4$ are in good agreement with the results of previous calculations.[42,43] In the present work, however, the FM solution for $CdCr_2S_4$ is insulating, whereas in Ref. 42, metallic FM solutions were obtained for both compounds. A possible cause for the difference is that in Ref. 42 structural data with the S fractional coordinate $x=1/4$ were used.

A Cr spin magnetic moment defined as a volume integral of the spin density over a Cr atomic sphere varies from

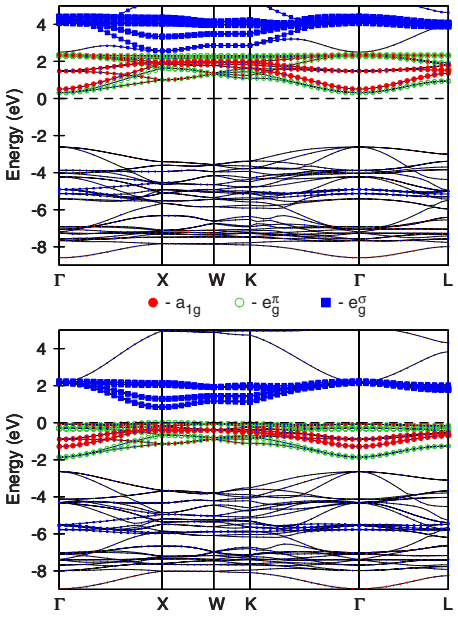

FIG. 6. (Color online) Majority- (lower panel) and minority-spin (upper panel) fat bands calculated for $ZnCr_2O_4$ with FM alignment of Cr magnetic moments. The size of filled (red) and hollow (green) circles and (blue) squares is proportional to the partial weight of Cr a_{1g}, e^{π}_{g}, and e^{σ}_{g} states in the Bloch wave function, respectively. Zero energy is chosen at the Fermi level.

$2.86\mu_B$ in $ZnCr_2O_4$ to $3.15\mu_B$ in $CdCr_2Se_4$, which agrees with a good accuracy with the value of $3\mu_B$ expected for the completely polarized t_{2g} shell filled with three electrons. The hybridization with Cr d states induces weak negative spin-polarization of $X\,p$ states. It is, however, partially compensated by a positive contribution coming from the "tails" of

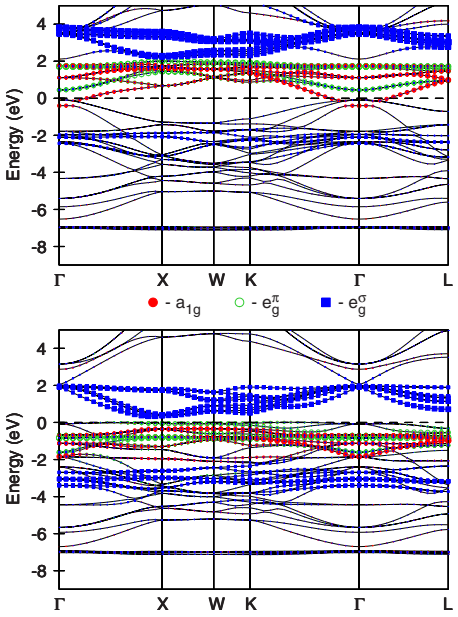

FIG. 7. (Color online) Majority- (lower panel) and minority-spin (upper panel) fat bands for $ZnCr_2Se_4$ (see caption of Fig. 6 for details).

Cr d states that have the d symmetry inside an X atomic sphere. The net spin magnetic moment M_X induced on X ions is small and negative with $M_O \approx -0.01\mu_B$, $M_S \approx -0.05\mu_B$, and $M_{Se} \approx -0.09\mu_B$. The moment induced on A ions is less than $0.05\mu_B$.

The self-consistent FM solution discussed above can be obtained for any of the nine spinels but it does not necessarily have the lowest total energy. If the coupling between Cr spins is AFM, then, because of geometrical frustrations intrinsic to the pyrochlore lattice formed by Cr ions, any configuration of classical spins such that the sum of four spin vectors sitting in the corners of each tetrahedron is equal to zero is the ground state of the Heisenberg Hamiltonian with nearest neighbor interactions.[4] The requirement of zero total spin in each tetrahedron is satisfied, for example, if Cr spins are aligned ferromagnetically along the $[1 \pm 10]$ chains and antiferromagnetically along $[01 \pm 1]$ and $[10 \pm 1]$ ones or, in other words, if Cr spins in each (001) plane are parallel but the spins in consecutive planes along the [001] direction are antiparallel to each other. In the following, this spin configuration will be denoted as AFZ. It is easy to check that in this case only four of six Cr-Cr bonds in each tetrahedron are AFM, while the other two remain FM and the magnetic energy cannot be minimized for all six bonds simultaneously if the coupling between Cr spins is antiferromagnetic.

Another spin configuration which gives zero total spin in each tetrahedron and does not break the cubic symmetry of the lattice is a noncollinear one with Cr spins directed along the lines passing through the center of a tetrahedron, i.e., along one of the $\langle 111 \rangle$ directions, with all four Cr spins pointing either to or away from the center. Self-consistent band structure calculations performed with this configuration of Cr spins gave for all the ACr_2X_4 spinels insulating solutions with zero net magnetic moment, which in the following is referred to as a ZM solution. Cr magnetic moments calculated in the local spin frame are about $0.1\mu_B$ smaller than for the corresponding FM solution but still close to $3\mu_B$. Depending on the magnetization directions of four Cr ions in a Cr_4X_4 cube, the magnetizations in four X atomic spheres are parallel or antiparallel to the vectors pointing to the center of the cube so that small X magnetic moments also cancel each other. With this arrangement of Cr and X moments, the spin moments of A ions are equal to zero. It is worth noting that for all the ACr_2X_4 compounds, the LSDA total energy difference between the AFZ and ZM solutions does not exceed 3 meV/f.u.

The comparison of the LSDA total energies of FM and ZM solutions shows that in $ZnCr_2O_4$ the solution with zero net moment is significantly more favorable, with the energy difference per f.u. being 171 meV. In $CdCr_2O_4$, this difference decreases to 19 meV, whereas in $HgCr_2O_4$, the two solutions are almost degenerate, the FM one being 2 meV lower. In the sulfides and selenides, the FM solution becomes more preferable. As Zn is replaced by a heavier ion, the energy difference between the two solution increases from 43 to 118 meV/f.u. in sulfides and from 80 to 134 meV/f.u. in selenides.

These results indicate that the change of the sign of dominant exchange interactions from AFM in oxides to FM in sulfides and selenides is captured already by LSDA band structure calculations. Moreover, all the compounds show a clear tendency to ferromagnetism as the lattice expands due to the increase of the radius of A ions.

C. Local spin-density approximation plus U results

In ACr_2X_4, as well as in many other $3d$ compounds, LSDA underestimates correlation effects in the rather localized Cr $3d$ shell. The strong electronic correlations can be accounted for, at least on a mean-field level, by using the LSDA+U approach. Since Cr t_{2g} states are split by the on-site exchange interaction into occupied majority- and unoccupied minority-spin states, charge and orbital degrees of freedom are frozen already in LSDA. As a consequence, LSDA+U band structures of the ACr_2X_4 spinels are qualitatively similar to the LSDA results.

When nonspherical terms of the Coulomb repulsion are neglected, the orbital dependent LSDA+U potential V_i can be approximated as $V_i = U'(1/2 - n_i)$, where n_i is the occupation of ith localized orbital, $U' = U - J_H$, and U is the effective screened Coulomb repulsion between $3d$ electrons. Taking into account that the orbital occupations n_i of Cr $t_{2g\uparrow}$ and $t_{2g\downarrow}$ states are close to 1 and 0, respectively, the main effect of the LSDA+U potential is to shift the $t_{2g\uparrow}$ states to lower and $t_{2g\downarrow}$ to higher energies by $U'/2$. Thus, the splitting between the $t_{2g\downarrow}$ and $t_{2g\uparrow}$ states increases from $3J_H$ in LSDA calculations to $3J_H + U'$ in LSDA+U ones. In oxides, because of the downward shift of the $t_{2g\uparrow}$ states, they start to overlap with O p bands. In $ACr_2S(e)_4$, the $t_{2g\uparrow}$ states move further below the top of X p bands and their contribution to the highest occupied majority-spin bands decreases. Due to the increase of the $t_{2g\downarrow} - t_{2g\uparrow}$ splitting, ferromagnetic LSDA+U solutions for all nine compounds considered in the present work become insulating starting from $U = 3$ eV.

Because of the strong Cr e_g^σ-X p hybridization discussed in Sec. IV A, the orbital occupations n_i calculated for the formally unoccupied Cr e_g^σ states are in the range of 0.28–0.48 for the majority- and about 0.22–0.25 for the minority-spin orbitals. As a result, the shift of the Cr e_g^σ states to higher energies caused by the Coulomb repulsion U is somewhat smaller than for the $t_{2g\downarrow}$ states for which n_i does not exceed 0.07 and the splitting between $e_{g\downarrow}^\sigma$ and $t_{2g\downarrow}$ states decreases with the increase of U.

V. EFFECTIVE EXCHANGE COUPLING CONSTANTS

Effective exchange coupling constants J_n between Cr spins were determined by performing band structure calculations for spiral spin structures with a varying wave vector $\mathbf{q}$. Then, the $\mathbf{q}$ dependence of the energy of the spin spirals was mapped onto a classical Heisenberg model. In order to get reliable estimates for J_n, one needs to perform calculations for a sufficiently large number of $\mathbf{q}$. Since self-consistent calculations for spin spirals are much more time consuming than conventional collinear spin-polarized calculations, the $\mathbf{q}$ dependence of their energy was calculated using the so-

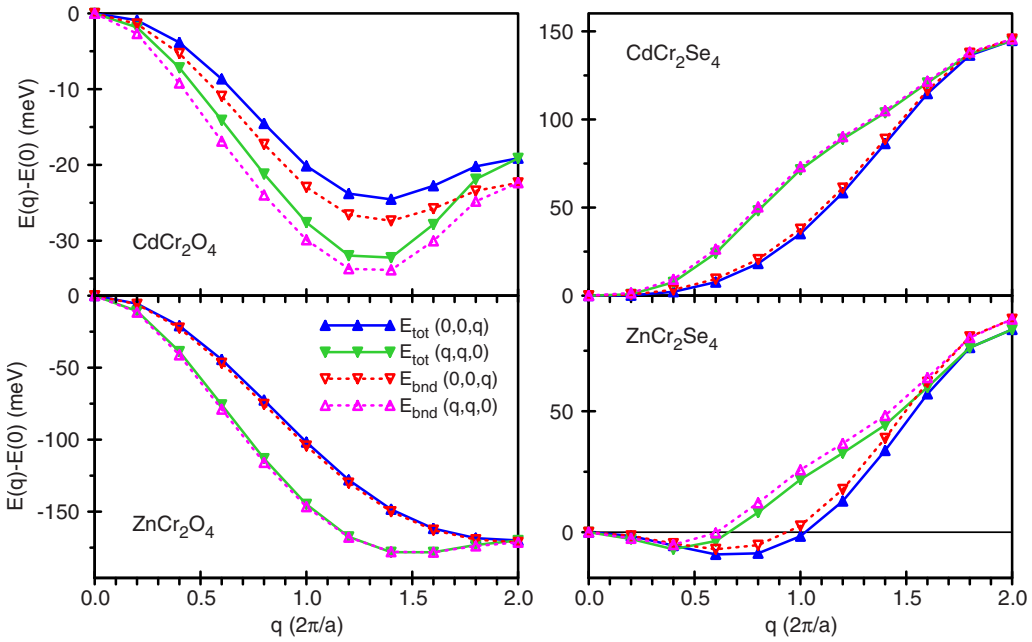

FIG. 8. (Color online) The dependence of the total $E_{tot}(\mathbf{q})$ and band $E_{bnd}(\mathbf{q})$ energies calculated within the LSDA on the wave vector of $(0,0,q)$ and $(q,q,0)$ spin spirals. The energies are plotted relative to the energy of the FM states with $q=0$.

called local force theorem (LFT).[44,45] According to this approach, the total energy difference between two spin configurations can be approximated by the difference of their band energies, provided that the calculations are performed starting from the same electron spin densities and only the magnetization direction varies. Strictly speaking, this approximation is justified only for small deviations of the magnetization direction from some collinear spin arrangement, i.e., for small $|\mathbf{q}|$, and before using it for short wavelengths, we have numerically checked its accuracy for the case of the ACr_2X_4 compounds.

First, self-consistent calculations were performed for two sets of planar spin spirals with the magnetization direction inside a Cr sphere fixed by polar angles $\theta=\pi/2$ and $\phi=\mathbf{q}\cdot(\mathbf{t}+\mathbf{R})$, where $\mathbf{t}$ is the position of a Cr site in the unit cell and $\mathbf{R}$ is a lattice vector. The wave vectors $\mathbf{q}=(0,0,q)$ and $\mathbf{q}=(q,q,0)$ of the spirals varied along the Γ-X and Γ-K high symmetry directions, respectively, in the range $0\leqslant q\leqslant 2$ in $2\pi/a_0$ units. Obviously, the (0,0,0) spiral is the collinear FM structure with the magnetization directed along the x axis, whereas (2,2,0) and (0,0,2) spirals are equivalent to the collinear AFZ spin structure with zero net magnetization discussed in Sec. IV B. The magnetization directions in other atomic spheres were determined self-consistently.

Then, band energies for the same spin spirals were calculated starting from self-consistent FM electron densities for $ACr_2S(e)_4$ and from the densities for the ZM solution in the case of oxides. When using LFT for spinels, one needs to specify the magnetization direction not only for magnetic Cr ions but also in A, X, and E spheres in which small but finite magnetic moments are induced. In a general case, this direction is not uniquely determined by $\mathbf{q}$ but instead depends in a nontrivial way on the orientation of Cr magnetic moments. We found that good agreement between the $\mathbf{q}$ dependencies of the total $E_{tot}(\mathbf{q})$ and band $E_{bnd}(\mathbf{q})$ energies can be obtained when the small exchange splitting in A, X, and E spheres is completely neglected. $E_{bnd}(\mathbf{q})$ curves calculated in this way for some of the Cr spinels are compared to $E_{tot}(\mathbf{q})$ in Fig. 8. Both energies are plotted relative to the energy of the FM solution with $q=0$. The difference between $E_{bnd}(\mathbf{q})$ and $E_{tot}(\mathbf{q})$ does not exceed 5 meV and is much smaller than the variation of the total energy with q even for $CdCr_2O_4$. Somewhat larger differences of about 8 meV are calculated for sulfides (not shown in Fig. 8). If the spin polarization inside non-Cr spheres was not switched-off and the magnetization directions obtained from self-consistent calculations were used in LFT calculations, slightly larger differences between the total and band energies were obtained. Below, when discussing exchange coupling constants between Cr spins, we will drop the subscript *bnd* and denote the band energy calculated with the spin polarization in A, X, and E spheres set to zero simply as $E(\mathbf{q})$.

The calculations for spin spirals confirm the conclusion, drawn in Sec. IV B on the base of comparison of the FM and ZM total energies, that the energy of the zero net moment solution $(q=2)$ is lower than the FM one $(q=0)$ in oxides, whereas in $ACr_2S(e)_4$, the FM solution becomes more stable. However, the shift of the minimum of $E(\mathbf{q})$ curves to intermediate values of q, most clearly seen for the Γ-K direction, witnesses that alongside geometrical frustrations there is also a competition between the nearest-neighbor exchange interaction and more distant ones. Only in $CdCr_2Se_4$ and $HgCr_2Se_4$, the minimum is at $q=0$ and the FM solution has the lowest energy.

Quantitative estimates for J_n up to the fourth shell of Cr neighbors were obtained by mapping the energy of spin spirals onto a classical Heisenberg model,

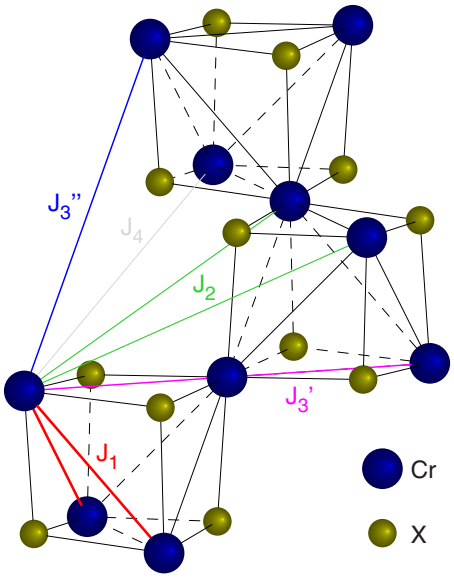

FIG. 9. (Color online) Exchange coupling constants J_n up to the fourth Cr neighbors.

$$E_H = \frac{1}{4}\sum_{i=1}^{4}\sum_{n=1}^{4}\sum_{j=1}^{z_n} J_n \mathbf{S}_i \cdot \mathbf{S}_j, \tag{4}$$

where i numbers Cr sites in the unit cell and j runs over z_n neighbors in the nth shell around the site i. Positive J_n correspond to AFM coupling between Cr spins. Note that an additional factor of $1/2$ appears in Eq. (4) because the magnetic energy is given per f.u. and there are 2 f.u. in the unit cell. The length of the Cr spins $\mathbf{S}_i$ was fixed to $3/2$. Then, $E_H(\mathbf{q})$ depends only on the angle between a pair of Cr spins which is uniquely determined by the wave vector $\mathbf{q}$ of a spiral provided that for four Cr ions at positions $\mathbf{t}_i$ in the unit cell the phases are fixed by $\phi_i = \mathbf{t}_i \cdot \mathbf{q}$.

Some pairs of Cr ions coupled by J_1-J_4 are shown in Fig. 9. Each Cr site has six first (J_1) and 12 second (J_2) neighbors at distances $a_0\sqrt{2}/4$ and $a_0\sqrt{6}/4$, respectively. The third shell consists of 12 Cr sites at $a_0\sqrt{2}/2$ which are split into two inequivalent sextets. The corresponding coupling constants are denoted as J_3' and J_3''. J_3' couples Cr sites which lie on one of the $\langle 110 \rangle$ chains and are actually the second Cr neighbors along the chain. Cr sites coupled by J_3'' belong to parallel Cr chains. For the spin spirals considered here, terms proportional to J_3' and J_3'' in Eq. (4) have the same $\mathbf{q}$ dependence so that it was not possible to separate their contributions to the magnetic energy and only their average $J_3 = (J_3' + J_3'')/2$ could be determined from the fit. We will return to the discussion of J_3' and J_3'' later. Finally, in the fourth shell, there are 12 Cr sites at the distance $a_0\sqrt{10}/4$ (J_4) which lie at the same chains as the second Cr neighbors.

In order to get reliable values of J_n, additional LFT calculations for spirals with wave vectors (q,q,q), $(1,q,0)$, and $(1,1,q)$ were performed. For the $(1,q,0)$ and $(1,1,q)$ spirals, the contributions to $E_H(\mathbf{q})$ proportional to J_3 and J_1, respectively, do not depend on q, which allows us to determine these coupling constants with higher accuracy. Explicit expressions for $E_H(q)$ for the above mentioned spin spirals are given in the Appendix.

The results of a simultaneous least-squares fit of $E_H(\mathbf{q})$ given by Eq. (4) to $E(\mathbf{q})$ calculated within LSDA along the five $\mathbf{q}$ directions are shown in Fig. 10 together with contributions to $E_H(\mathbf{q})$ coming from different nearest neighbors shells (E_n). The values of J_n obtained from the fit are collected in Table II. The dominant contribution to $E_H(\mathbf{q})$ is provided by the nearest-neighbor coupling J_1 which is AFM in ACr_2O_4 and FM in $ACr_2S(e)_4$. In oxides, however, the strength of AFM J_1 decreases dramatically with the increase of the A ionic radius: in $CdCr_2O_4$, J_1 is more than five times weaker than in $ZnCr_2O_4$, while in $HgCr_2O_4$, it becomes almost zero. In $ACr_2S(e)_4$, the strength of FM J_1 tends to increase in the row Zn→Cd→Hg but the changes are not as strong as in the oxides, with the values of J_1 calculated for the Cd and Hg compounds being comparable.

Another significant contribution to $E_H(\mathbf{q})$ comes from the term proportional to J_3 which is AFM in all the ACr_2X_4 spinels considered in the present work. It is the competition between the J_1 and J_3 terms which shifts the minimum of the $(0,0,q)$ and $(q,q,0)$ curves to incommensurate $\mathbf{q}$ vectors. For $\mathbf{q}=(0,0,q)$, $E_H(\mathbf{q})$ has the same q dependence as a linear chain of classical spins with competing nearest $J=J_1$ and next-nearest $J'=2J_3$ neighbor interactions. The ground state of such a chain becomes incommensurate if the ratio J'/J is larger than the critical value of 0.25. Since J_3 is not very sensitive to the size of A ion, the ratio $2J_3/J_1$, which is less than 0.1 in $ZnCr_2O_4$, increases to 0.45 in $CdCr_2O_4$, while in the Hg oxide J_3 becomes the dominant magnetic interaction. The values of J_3 calculated for $ACr_2S(e)_4$ are more than two times larger than in the oxides. The largest $|2J_3/J_1|$ ratios of 0.75 and 0.48 are found for $ZnCr_2S_4$ and $ZnCr_2Se_4$, in which the FM nearest-neighbor interaction is the weakest. In other two selenides, $|2J_3/J_1| \approx 0.26$ is only slightly larger than the critical value of 0.25.

According to the results of the least-square fit, the exchange interactions between the second and fourth Cr neighbors are much weaker than J_1 and J_3. While the sign of J_2 varies form one compound to another, J_4 is always ferromagnetic and somewhat larger in sulfides and selenides compared to oxides.

The reliability of the fitted J_n was checked by comparing the values obtained from the fit to the band energies calculated for all five spin spirals ($J_n^{(5)}$) to those fitted to $(0,0,q)$ and $(q,q,0)$ results only ($J_n^{(2)}$). In the case of J_1, the relative uncertainty of the determination of J_n, defined as $\delta_n = |J_n^{(5)} - J_n^{(2)}|/J_n^{(5)}$, is less than 1%, except for $HgCr_2O_4$ where J_1 itself is very small. The uncertainty in J_3 values is about 1% in $ACr_2S(e)_4$ and 10% in oxides. The values of $\delta_2 \sim 5\%$ and $\delta_4 \sim 10\%$ are also smaller in $ACr_2S(e)_4$ than in the oxides, in which they are about 30%. The largest uncertainties in the LSDA values of $J_2 - J_4$ were found in the case of $ZnCr_2O_4$. A plausible reason is that the nearest-neighbors terms of the order of $(\mathbf{S}_i \cdot \mathbf{S}_j)^2$ in the expansion of the magnetic energy[46] may become comparable to the contribution of weak couplings between distant Cr neighbors. Neither the fitted values of J_n nor the quality of the fit were noticeably affected if exchange couplings between fifth Cr neighbors were in-

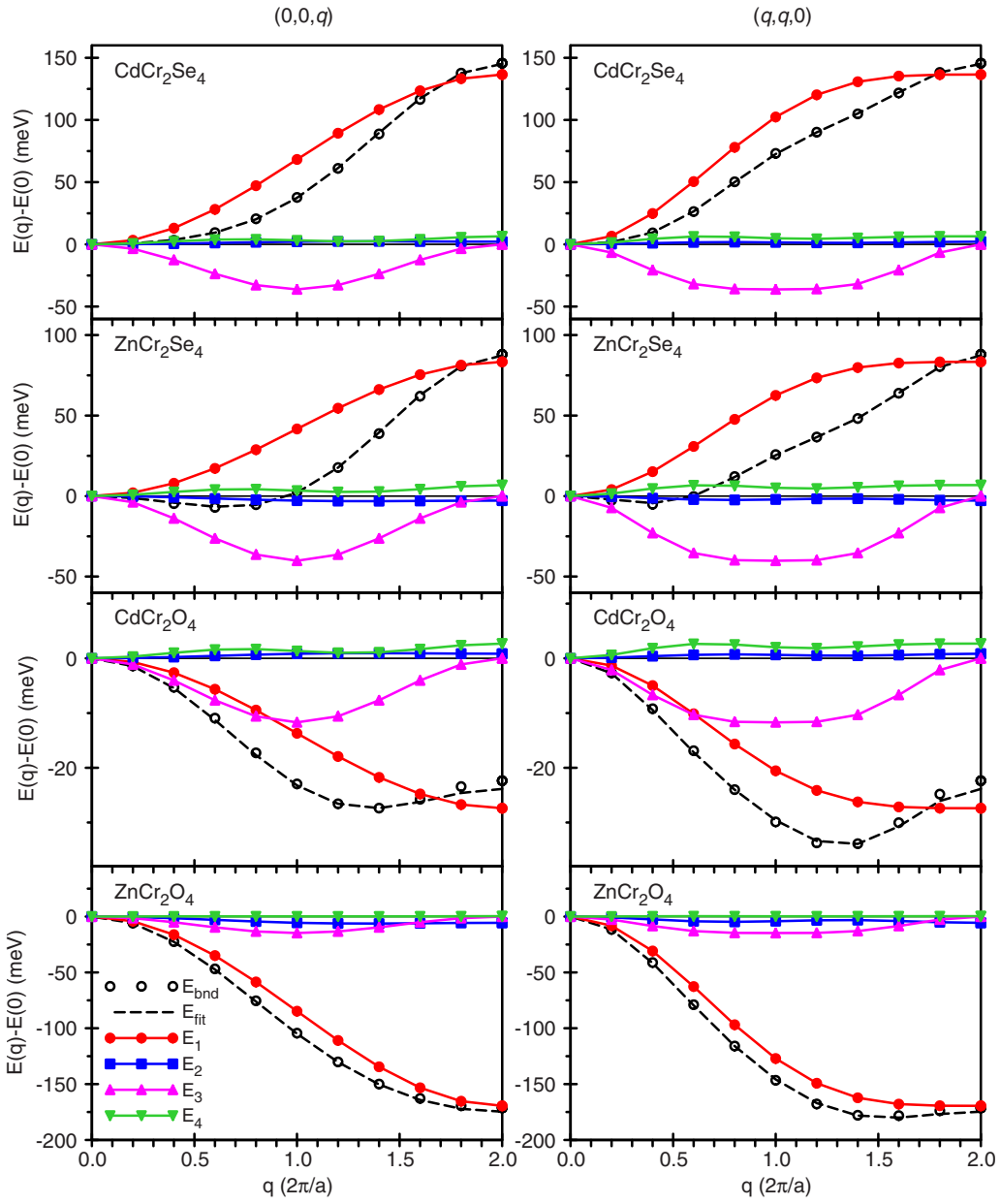

FIG. 10. (Color online) The comparison of calculated band energies (E_{bnd}) and the results of the fit using Eq. (4) (E_{fit}) for $\mathbf{q}=(0,0,q)$ (left panels) and $\mathbf{q}=(q,q,0)$ (right panels). Individual contributions E_n of the terms proportional to J_n are also plotted.

cluded into the fit. Accounting for more distant sixth neighbors allowed us to decrease the mean deviation between the calculated and fitted energies for $ACr_2S(e)_4$ but the obtained values of J_6 were even smaller than J_2 and J_4 and could not be determined reliably. Finally, significantly smaller values of δ_n were obtained when fitting $E_H(\mathbf{q})$ to LSDA+U band energies.

J_n obtained by fitting $E_H(\mathbf{q})$ to band energies calculated using the LSDA+U approach with $U=2$, 3, and 4 eV are presented in Table III. Both J_1 and J_3 derived from the LSDA+U calculations with $U=2$ eV for ACr_2O_4 are weaker than the corresponding LSDA values. The only exception is $HgCr_2O_4$, in which J_1 is weakly FM in LSDA and becomes somewhat stronger in LSDA+U. In $ZnCr_2O_4$, the value of J_1 rapidly decreases with the increase of U as it is expected if $J \sim t^2/U$. In Cd and Hg spinels, on the other hand, the increase of U tends to make J_1 more ferromagnetic. It looks as if there were two competing contributions of the opposite signs to J_1: as the AFM one is suppressed by U the ferromagnetic contribution wins. Comparable values of $J_1=0.5$ meV, $J_2 \approx 0$ meV, and $J_3=0.15$ meV were obtained from LSDA+U calculations for $CdCr_2O_4$ in Ref. 21. These calculations, however, were performed using theoretical lattice parameters.

In $ZnCr_2S_4$, $|J_1|$ calculated with $U=2$ eV is slightly larger than the LSDA value and continue to increase with the increase of U, whereas in $ZnCr_2Se_4$, J_1 is practically independent of U. In other $ACr_2S(e)_4$ spinels, switching on U suppresses J_1 but the increase of U from 2 to 4 eV has only minor effect on its strength.

TABLE II. Exchange coupling constants J_n/k_B (K) and Θ_{CW} (K) obtained from the least-squares fit of $E_H(\mathbf{q})$ given by Eq. (4) to the energy of spin spirals calculated within LSDA.

	J_1/k_B	J_2/k_B	J_3/k_B	J_4/k_B	Θ_{CW}
$ZnCr_2O_4$	109	1.8	4.8	−0.1	−916
$CdCr_2O_4$	18	−0.3	3.8	−0.9	−172
$HgCr_2O_4$	−1	1.8	5.4	−0.8	−92
$ZnCr_2S_4$	−37	2.8	13.8	−1.5	49
$CdCr_2S_4$	−74	0.6	12.0	−1.7	392
$HgCr_2S_4$	−86	2.8	13.3	−1.7	432
$ZnCr_2Se_4$	−54	0.9	13.0	−2.2	228
$CdCr_2Se_4$	−88	−0.7	11.7	−2.1	526
$HgCr_2Se_4$	−86	0.0	11.6	−2.6	509

In all the compounds, J_3 obtained from the LSDA+U calculations is AFM and weaker than in LSDA. In ACr_2O_4 and ACr_2S_4, its value decreases with the increase of U, while in selenides, its U dependence is very weak. J_2 remains vanishingly small but shows clear tendency to become more FM as U increases. Finally, in ACr_2O_4 and ACr_2Se_4, the increase of U affects J_4 in opposite ways: In oxides, the strength of FM J_4 increases, whereas in selenides, $|J_4|$ decreases and for $U=4$ eV, it changes sign.

In order to separate J_3' and J_3'' contributions to $E_H(\mathbf{q})$, we performed calculations for noncollinear spin superstructures in which Cr moments only in every second (001) plane, the one that contains [110] Cr chains, are oriented in the ab plane, with their directions being determined as before by $\theta=\pi/2$ and $\phi=\mathbf{q}\cdot(\mathbf{t}+\mathbf{R})$. Cr moments in other planes, which contain $[1\bar{1}0]$ chains, are aligned parallel to the c axis ($\theta=0$) so that their directions do not depend on ϕ and, consequently, on $\mathbf{q}$. In this case, the third Cr neighbors in the ab plane that lie on the same [110] chain (J_3') and on parallel chains (J_3'') give different contributions to the q dependence of the energy of $(q,q,0)$ and $(q,-q,0)$ spin spirals, which allows us to determine J_3' and J_3'' separately provided that other J_n are known. Calculations performed for ACr_2O_4 and ACr_2Se_4 show that J_3' and J_3'' are of comparable strengths. The calculated J_3''/J_3' ratio is 0.6, 0.5, and 1.1 in Zn, Cd, and Hg oxides, respectively, while for the selenides, the values of 0.8, 0.8, and 1.0 were obtained. It seems plausible that the contribution of Hg 6s states to Cr d-X p-Cr d hybridization is responsible for somewhat larger values of J_3'' in the Hg compounds.

It should be mentioned that the values of J_n presented in Table III are somewhat different from the preliminary results published in Ref. 47 for the following reasons: (i) for $CdCr_2O_4$, old structural data from Ref. 48 with the O fractional coordinate $x=0.260$, which seems to be too small, were used, (ii) the calculations for oxides in Ref. 47 were performed with O s and p states only included in the LMTO basis set (this gives smaller values of J_1 compared to the present calculations in which O d are also included into the basis) and (iii) the calculations in Ref. 47 were performed for $(q,q,0)$ and $(0,0,q)$ spirals only and the coupling constants between third Cr neighbors along the ⟨110⟩ chains were included into the fit instead of J_4. Later, it was verified that accounting for true J_4 to fourth Cr neighbors improves the quality of the fit and seems more physical. We have to stress, however, that despite the differences in calculated values of J_n the main conclusions of Ref. 47 concerning the relative strengths of various exchange interactions and their origins remain unaffected.

TABLE III. Exchange coupling constants J_n/k_B (K) and Θ_{CW} (K) obtained from the least-squares fit of $E_H(\mathbf{q})$ given by Eq. (4) to the energy of spin spirals calculated using the LSDA+U approach with $U=2$, 3, and 4 eV.

ACr_2X_4	U (eV)	J_1/k_B	J_2/k_B	J_3/k_B	J_4/k_B	Θ_{CW}
$ZnCr_2O_4$	2	61	0.3	2.9	−0.3	−500
	3	40	0.0	2.3	−0.4	−328
	4	25	−0.2	1.9	−0.5	−209
$CdCr_2O_4$	2	6	−0.3	2.2	−0.4	−64
	3	−4	−0.4	1.7	−0.4	12
	4	−9	−0.4	1.4	−0.4	62
$HgCr_2O_4$	2	−7	1.2	3.3	0.0	−14
	3	−14	0.6	2.4	−0.1	59
	4	−18	0.3	1.9	−0.2	104
$ZnCr_2S_4$	2	−43	1.7	8.5	−0.6	175
	3	−48	0.8	7.2	−0.8	267
	4	−52	0.1	6.4	−0.7	306
$CdCr_2S_4$	2	−62	0.4	7.2	−0.9	367
	3	−65	−0.2	6.2	−0.9	416
	4	−66	−0.6	5.7	−0.7	433
$HgCr_2S_4$	2	−72	1.6	8.0	−0.9	412
	3	−74	0.5	6.6	−0.9	464
	4	−74	−0.2	5.8	−0.7	481
$ZnCr_2Se_4$	2	−49	0.5	8.3	−0.9	246
	3	−52	−0.5	7.8	−0.6	286
	4	−52	−1.1	8.1	0.0	286
$CdCr_2Se_4$	2	−70	−0.5	7.1	−0.9	432
	3	−69	−1.1	7.1	−0.4	434
	4	−67	−1.4	7.6	0.2	410
$HgCr_2Se_4$	2	−69	−0.1	7.5	−0.9	422
	3	−68	−1.0	7.2	−0.2	420
	4	−66	−1.4	7.8	1.1	384

VI. DISCUSSION

The effective Curie–Weiss temperatures estimated from the calculated J_n according to

$$\Theta_{CW}=\frac{S(S+1)}{3}\sum_n z_n J_n, \tag{5}$$

with $S=3/2$ are given in the last column of Tables II and III. The comparison of the estimated Θ_{CW} to experimental values

from Ref. 2 (Table I) shows that the LSDA calculations reproduce the opposite signs of Θ_{CW} in ACr_2O_4 and $ACr_2S(e)_4$ but strongly overestimate its magnitude, which is not surprising as one can expect that LSDA underestimates correlation effects in the rather localized Ce $3d$ shell. Since the absolute values of Θ_{CW} calculated for oxides rapidly decrease with the increase of U in the LSDA+U calculations, it is possible to adjust the value of U so as to reproduce the experimental Θ_{CW}. This, however, would require to use different values of U for the Zn, Cd, and Hg oxospinels. In $ACr_2S(e)_4$, the estimated values of Θ_{CW}, which are too high already in LSDA, further increase when the LSDA+U approach is used. As the dominant contribution to Θ_{CW} is provided by J_1, it seems that the tendency to ferromagnetic coupling between nearest Cr neighbors is overestimated in the LSDA+U calculations.

The comparison of the calculated J_n to experimental estimates for the exchange coupling constants in $ZnCr_2S_4$ (J_1 =2.66 K, J_2=−1.15 K, J_3=0.29 K, and J_4=0.13 K)[12] and $CdCr_2S_4$ (J_1=13.25 K and J_3=−0.915 K)[49] also shows that the calculations overestimate the strength of the exchange interactions between Cr spins. Note that the experimental values of J_n should be multiplied by a factor of 2 because of the different definitions of the magnetic energy [see Eq. (2) in Ref. 12], while their signs should be inverted since in Refs. 12 and 49 the positive sign of J_n corresponds to FM coupling. Also it is worth mentioning that J_n are not directly measurable quantities and in order to determine them from experimental data additional assumption should be made. The experimental wave vector $\mathbf{q}_{exp}=(0,0,0.79)$ of the helimagnetic structure in $ZnCr_2S_4$ is very close to $\mathbf{q}_{min}=(0,0,0.82)$ at which the LSDA energy of the $(0,0,q)$ spin spiral has a minimum. Under assumption that J_2 and J_4 are much smaller than J_1 and J_3, this gives the J_1/J_3 ratios of 0.39 and 0.37 in the experiment and theory, respectively. For $ZnCr_2Se_4$, LSDA gives the minimum of $E(q)$ along the Γ-X at $\mathbf{q}_{min}=(0,0,0.65)$ which is larger than the experimental wave vector $\mathbf{q}_{expt}=(0,0,0.466)$.[11] In the LSDA+$U$ calculations, however, the minimum shifts toward smaller q values.

In order to understand better the dependence of the calculated exchange coupling constants on the chemical composition and on the value of the parameter U in LSDA+U calculations, let us for simplicity consider a pair of Cr^{3+} ions with occupied $t_{2g\uparrow}$ states at zero energy, unoccupied $t_{2g\downarrow}$ states at the energy $\Delta_{\uparrow\downarrow}$, and an effective t_{2g}-t_{2g} hopping matrix element t. The splitting $\Delta_{\uparrow\downarrow}$ is close to $3J_H$ in the LSDA and $3J_H+U'$ in the LSDA+U calculations. Cr e_g^σ states with both spin projections are unoccupied and also split by $\Delta'_{\uparrow\downarrow}$ which in LSDA is equal to $3J_H$. The LSDA energy difference Δ_{e-t} between e_g^σ and t_{2g} states with the same spin projections is equal to the crystal field splitting Δ_{CF} which is of the same order as $\Delta'_{\uparrow\downarrow}$ as is evidenced by the results presented in Sec. IV B.

Hybridization, either direct or indirect via $X\,p$ states, between the half-filled Cr t_{2g} states results in AFM exchange coupling provided that the t_{2g} bandwidth is less than $\Delta_{\uparrow\downarrow}$. Indeed, if Cr moments are aligned ferromagnetically, the hybridization between the t_{2g} states gives no gain in the kinetic energy as in the majority-spin channel both bonding and antibonding combinations with energies $\varepsilon_\uparrow^b=-t$ and $\varepsilon_\uparrow^{ab}=t$ are occupied, whereas in the minority-spin channel, both of them ($\varepsilon_\downarrow^{b,ab}=\Delta_{\uparrow\downarrow}\pm t$) are empty (see Fig. 11). If the magnetizations of two Cr ions are antiparallel, an occupied $t_{2g\uparrow}$ state can hybridize only with the unoccupied t_{2g} state with the same spin projection of another ion lying at the energy $\Delta_{\uparrow\downarrow}$. In this case, only their bonding combination with the energy $\varepsilon_\uparrow^b\approx -t^2/\Delta_{\uparrow\downarrow}$ is occupied. Since the energy of the bonding state with the opposite spin projection is exactly the same, this gives

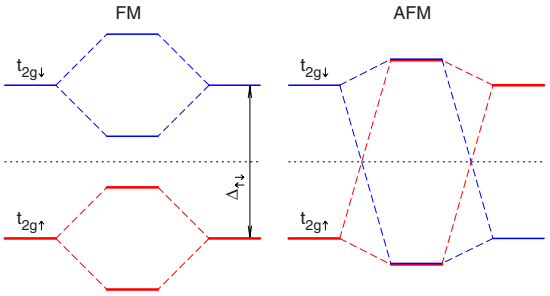

FIG. 11. (Color online) A sketch of bonding and antibonding states between Cr t_{2g} state for FM (left) and AFM (right) alignments of Cr magnetizations. The Fermi level is plotted by a horizontal dotted line.

$$E_{FM}-E_{AFM}\equiv 2J_{AFM}S^2\approx 2t^2/\Delta_{\uparrow\downarrow} \tag{6}$$

for the energy difference of the FM and AFM configurations.

Cr e_g states with both spin projections are unoccupied and t_{2g}-e_g^σ hybridization (t') lowers the energy of the FM as well as AFM configuration because in both cases only the bonding combination is occupied (see Fig. 12). The energy of the bonding state $\varepsilon_\uparrow^b\approx -t'^2/(\varepsilon_{e_g}-\varepsilon_{t_{2g}})$ is, however, lower if the magnetizations of two Cr ions are parallel. In this case, the e_g^σ partner with the same spin as the occupied t_{2g} state has lower energy $\varepsilon_{e_g}=\Delta_{e-t}$ vs $\varepsilon_{e_g}=\Delta_{e-t}+\Delta'_{\uparrow\downarrow}$ in the AFM case, so that

$$E_{FM}-E_{AFM}\equiv 2J_{FM}S^2\approx -\frac{2t'^2\Delta'_{\uparrow\downarrow}}{\Delta_{e-t}(\Delta_{e-t}+\Delta'_{\uparrow\downarrow})}, \tag{7}$$

and the effective coupling J_{FM} is ferromagnetic. It should be mentioned that these estimates for the effective exchange

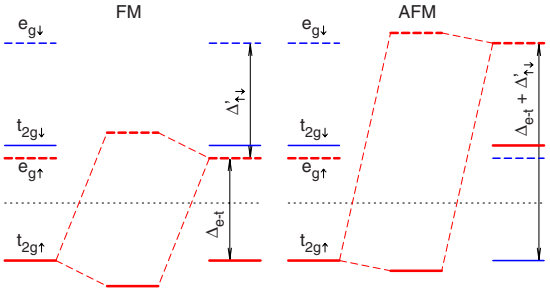

FIG. 12. (Color online) A sketch of bonding and antibonding states between an occupied Cr $t_{2g\uparrow}$ state and an unoccupied e_g^σ state with the same spin projection for FM (left) and AFM (right) alignments of Cr magnetizations. The Fermi level is plotted by a horizontal dotted line.

couplings are in agreement with the well known Goodenough–Kanamori rules.[19]

Thus, the strength and even the sign of J_1 in ACr_2X_4 are determined by the competition of two contributions of opposite signs, J_{AFM} and J_{FM}, which depend on the strength of the t_{2g}-t_{2g} and t_{2g}-e_g hybridizations, respectively. In $ZnCr_2O_4$, J_{AFM} dominates because of the strong direct hopping of $dd\sigma$ type between the Cr t_{2g} states. This conclusion has been confirmed numerically by the results of test LSDA calculations in which the hybridization between Cr d states was switched off. J_1 derived from a fit to band energies calculated in this way is about 1 K, whereas for other J_n, the values comparable to those given in Table II were obtained. With the increase of the lattice constant in the row Zn→Cd→Hg, the strength of the direct d-d hopping and, as a consequence, of J_{AFM} rapidly decreases so that in $HgCr_2O_4$ according to the LSDA results J_{AFM} and J_{FM} almost exactly compensate each other. The dependence of J_1 on the value of the parameter U in the LSDA+U calculations can be explained by weakening of J_{AFM} caused by the increase of the denominator in Eq. (6) which in this case is given by $\Delta_{\uparrow\downarrow} \approx 2J_H + U$.

In $ACr_2S(e)_4$ spinels, the distance between Cr nearest neighbors (see Table I) is much larger than in ACr_2O_4 and the contribution of the direct t_{2g}-t_{2g} hopping to J_1 becomes less significant. For $ZnCr_2Se_4$, for instance, calculations with switched-off Cr d-d hybridization give the value of FM J_1 which is only 5% larger than the LSDA one. Thus, the indirect hybridization via X p states between the half-filled t_{2g} and empty e_g states split by the on-site exchange interaction provides the dominant contribution to FM J_1 as was proposed by Goodenough in Ref. 18. A direct numerical proof is provided by test calculations in which an external orbital-dependent potential V_{eg} was added to Cr $e^{\sigma}_{g\uparrow}$ states, with its strength $V_{eg} \approx 3J_H$ being equal to the LSDA exchange splitting of the e^{σ}_g states. Then, the energies of Cr e^{σ}_g states with both spin projections are equal so that $\Delta'_{\uparrow\downarrow} \approx 0$ and the nominator in expression (7) for J_{FM} becomes zero. $J_1 = 15$ K estimated from such calculations for $ZnCr_2Se_4$ changes its sign to AFM and its absolute value is significantly smaller than $|J_1| = 54$ K obtained from the LSDA calculations. This indicates that the indirect t_{2g}-X p-t_{2g} hybridization also contribute to J_1 but it is much weaker than J_{FM}. Similar calculations for $ZnCr_2O_4$ result in substantial increase of the strength of AFM J_1 which means the FM contribution is present also in oxides but J_{AFM} wins due to direct d-d hybridization.

In order to explain the weird behavior of J_1 in LSDA+U calculations, one needs to analyze in more details various parameters entering Eq. (7). Recalling that the orbital dependent part of the LSDA+U potential can be approximated as $V_i = U'(1/2 - n_i)$ with $U' = U - J_H$, one gets

$$\Delta'_{\uparrow\downarrow} = 3J_H + U'(n_\uparrow - n_\downarrow), \tag{8}$$

$$\Delta_{e-t} = \Delta_{CF} + U'(1 - n_\uparrow), \tag{9}$$

where $n_\uparrow$ and $n_\downarrow$ are the occupation numbers of $e^{\sigma}_{g\uparrow}$ and $e^{\sigma}_{g\downarrow}$ states, respectively. Here, we neglected the small (~ 0.05) deviation of the occupation numbers of the minority-spin t_{2g} states from unity. Then, Eq. (7) can be written as

$$2J_{FM}S^2 \approx -\frac{2t'^2[3J_H + U'(n_\uparrow - n_\downarrow)]}{\Delta_{CF} + U'(1 - n_\uparrow)} \frac{1}{\Delta_{CF} + U'(1 - n_\downarrow) + 3J_H}. \tag{10}$$

If the occupations of the Cr e^{σ}_g were equal to zero, Eq. (10) would become

$$2J_{FM}S^2 \approx -\frac{6t'^2 J_H}{(\Delta_{CF} + U')(\Delta_{CF} + U' + 3J_H)}, \tag{11}$$

which would lead to fast decrease of J_{FM} with the increase of U'. However, since $n_\uparrow \sim 0.45$ and $n_\downarrow \sim 0.25$ were calculated for $ACr_2S(e)_4$, the appearance of the term proportional to $U'(n_\uparrow - n_\downarrow)$ in the nominator of Eq. (10) slows down the decrease of J_{FM}. Also the terms proportional to $n_\uparrow$ and $n_\downarrow$ in the dominator of Eq. (11) effectively decrease U', thus leading to the increase of J_{FM} as compared to purely ionic model with zero occupations of the e^{σ}_g states. This is one of possible reasons why the FM contribution to J_1 in overestimated in the LSDA+U calculations.

The calculated behavior of J_2, J_3, and J_4 follows the predictions made by Dwight and Menyuk [19,20] on the base of the Goodenough–Kanamori rules of superexchange.[16,17] Hybridization paths Cr d-X p-X p-Cr d responsible for these interactions include an intermediate hopping between p states of two X ions. This reduces the strength of the superexchange interactions but does not change the signs of t_{2g}-t_{2g} and t_{2g}-e_g contributions to J_n, which remain antiferromagnetic and ferromagnetic, respectively. Indirect t_{2g}-t_{2g} and t_{2g}-e_g hoppings give comparable contributions to J_2. Being of opposite signs, these contributions compensate each other. This explains the smallness of J_2 and the variation of its sign in the ACr_2X_4 spinels. Similar hybridization paths between d states of third neighbors, with the dominant contribution of the indirect t_{2g}-t_{2g} hopping, lead to the appearance of AFM J'_3 and J''_3. In the real structure, the distance between the pair of X ions along the J'_3 path is smaller than along the J''_3 one, the difference being proportional to the deviation of the positional parameter x from 1/4. This may explain why the calculated values of J'_3 are somewhat larger than J''_3. On the other hand, since the J''_3 pair of X ions belongs to the same AX_4 tetrahedron, J''_3 is more sensitive to A s-X p hybridization, which may be responsible for the increase of the J''_3/J'_3 ratio in the Hg-containing spinels. Finally, indirect hybridization between t_{2g} and e_g states gives dominant contribution to the superexchange between fourth neighbors[19] which leads to FM J_4.

VII. SUMMARY AND CONCLUSIONS

The LSDA(+U) band structure calculations performed for some ACr_2X_4 spinels reproduce the change of the sign of the nearest-neighbor exchange interaction between Cr spins from AFM in ACr_2O_4 compounds to FM in $ACr_2S(e)_4$ ones. It has been verified that the strength and the sign of J_1 depend on relative strengths of two contributions of opposite signs, AFM and FM, which are due to Cr t_{2g}-t_{2g} and t_{2g}-e_g hybridizations, respectively. In $ZnCr_2O_4$ J_{AFM} dominates because of the strong direct hopping between the Cr t_{2g} states.

As Zn is replaced by Cd or Hg, the strength of the direct hopping rapidly decreases with the increase of the Cr-Cr separation. As a result, J_1 in the corresponding oxides is much weaker than in $ZnCr_2O_4$. In the $ACr_2S(e)_4$ spinels, the FM contribution originating from the indirect hopping between half-filled t_{2g} and empty e_g states, split by the on-site exchange interaction, becomes dominant. However, the magnitude of the FM contribution to J_1 seems to be overestimated by the calculations. The strongest among more distant exchange couplings are J_3' and J_3'' to two sextets of third Cr neighbors. These interactions are always AFM and of comparable strengths. The couplings to second and fourth Cr neighbors are significantly weaker than J_1 and J_3. The obtained results are in accordance with the analysis of the exchange couplings in Cr spinels based on the Goodenough–Kanamori rules of superexchange and may be helpful for understanding the magnetic properties not only of Cr spinels but also Ti ($MgTi_2O_4$) and V (ZnV_2O_4, CdV_2O_4) ones, in which orbital degrees of freedom come into play.[50–52]

ACKNOWLEDGMENTS

The author is grateful to P. Fulde, N. Shannon, K. Penc, and V. Antonov for many helpful discussions and to H. Ueda for providing recent experimental data on the crystal structures of $CdCr_2O_4$ and $HgCr_2O_4$ spinels.

APPENDIX

Below explicit expressions for the difference $E_H(\mathbf{q}) - E_H(0)$, where $E_H(\mathbf{q})$ is given by Eq. (4) and

$$E_H(0) = 6J_1 + 12J_2 + 6J_3 + 12J_4, \tag{A1}$$

are written as a functions of the angle $\phi = q\pi/2$ for some directions of the wave vector $\mathbf{q}$ of spin spirals,

$\mathbf{q}=(0,0,q)$ $(\Gamma - X)$:

$$E(\phi) = 4J_1(\cos\phi - 1) + 4J_2(2\cos\phi + \cos 2\phi - 3) + 8J_3(\cos 2\phi - 1) + 4J_4(\cos\phi + \cos 3\phi - 2), \tag{A2}$$

$\mathbf{q}=(q,q,0)$ $(\Gamma - K)$:

$$E(\phi) = J_1(4\cos\phi + \cos 2\phi - 5) + 2J_2(2\cos\phi + \cos 2\phi + 2\cos 3\phi - 5) + 2J_3(4\cos 2\phi + \cos 4\phi - 5) + 2J_4(2\cos\phi + \cos 2\phi + 2\cos 3\phi + \cos 4\phi - 6), \tag{A3}$$

$\mathbf{q}=(q,q,q)$ $(\Gamma - L)$:

$$E(\phi) = 3J_1(\cos 2\phi - 1) + 3J_2(2\cos 2\phi + \cos 4\phi - 3) + 6J_3(\cos 4\phi - 1) + 6J_4(\cos 2\phi + \cos 4\phi - 2), \tag{A4}$$

$\mathbf{q}=(1,q,0)$:

$$E(\phi) = 2J_1(\cos\phi - 3) - 4J_2(\cos\phi + 3) - 16J_3 + 2J_4(\cos\phi + \cos 3\phi - 6), \tag{A5}$$

$\mathbf{q}=(1,1,q)$:

$$E(\phi) = -6J_1 - 12J_2 - 8J_3(\cos 2\phi + 1) - 12J_4. \tag{A6}$$

Here, $J_3 = (J_3' + J_3'')/2$ is the average of the exchange coupling constants for two inequivalent groups of third Cr neighbors.

[1] P. K. Baltzer, P. Wojtowicz, M. Robbins, and E. Lopatin, Phys. Rev. **151**, 367 (1966).
[2] T. Rudolf, C. Kant, F. Mayr, J. Hemberger, V. Tsurkan, and A. Loidl, New J. Phys. **9**, 76 (2007).
[3] A. P. Ramirez, Annu. Rev. Mater. Sci. **24**, 453 (1994).
[4] R. Moessner and J. T. Chalker, Phys. Rev. B **58**, 12049 (1998).
[5] S.-H. Lee, C. Broholm, T. H. Kim, W. Ratcliff, and S. W. Cheong, Phys. Rev. Lett. **84**, 3718 (2000).
[6] H. Ueda, H. A. Katori, H. Mitamura, T. Goto, and H. Takagi, Phys. Rev. Lett. **94**, 047202 (2005).
[7] J.-H. Chung, M. Matsuda, S.-H. Lee, K. Kakurai, H. Ueda, T. J. Sato, H. Takagi, K.-P. Hong, and S. Park, Phys. Rev. Lett. **95**, 247204 (2005).
[8] H. Ueda, H. Mitamura, T. Goto, and Y. Ueda, Phys. Rev. B **73**, 094415 (2006).
[9] K. Penc, N. Shannon, and H. Shiba, Phys. Rev. Lett. **93**, 197203 (2004).
[10] H. Ueda, J.-I. Yamaura, H. Mitamura, T. Goto, H. A. Katori, H. Takagi, and Y. Ueda, J. Magn. Magn. Mater. **310**, 1275 (2007).
[11] J. Akimitsu, K. Siratori, G. Shirane, M. Iizumi, and T. Watanabe, J. Phys. Soc. Jpn. **44**, 172 (1978).
[12] M. Hamedoun, A. Hourmatallah, S. Sayouri, and A. Chatwiti, J. Phys.: Condens. Matter **7**, 5359 (1995).
[13] J. Hemberger, T. Rudolf, H.-A. Krug von Nidda, F. Mayr, A. Pimenov, V. Tsurkan, and A. Loidl, Phys. Rev. Lett. **97**, 087204 (2006).
[14] J. Hemberger, P. Lunkenheimer, R. Fichtl, H.-A. Krug von Nidda, V. Tsurkan, and A. Loidl, Nature (London) **434**, 364 (2005).
[15] S. Weber, P. Lunkenheimer, R. Fichtl, J. Hemberger, V. Tsurkan, and A. Loidl, Phys. Rev. Lett. **96**, 157202 (2006).
[16] J. B. Goodenough, J. Phys. Chem. Solids **6**, 287 (1958).
[17] J. Kanamori, J. Phys. Chem. Solids **10**, 87 (1959).
[18] J. B. Goodenough, J. Phys. Chem. Solids **30**, 261 (1969).
[19] K. Dwight and N. Menyuk, J. Appl. Phys. **39**, 660 (1968).
[20] K. Dwight and N. Menyuk, Phys. Rev. **163**, 435 (1967).
[21] G.-W. Chern, C. J. Fennie, and O. Tchernyshyov, Phys. Rev. B **74**, 060405(R) (2006).
[22] H. Sawada, Mater. Res. Bull. **32**, 873 (1997).
[23] E. Riedel and E. Horvath, Z. Anorg. Allg. Chem. **371**, 248 (1969).
[24] T. N. Borovskaya, L. A. Butman, V. G. Tsirelson, M. A. Poraikoshits, T. G. Aminov, and R. P. Ozerov, Kristallografiya **36**, 612 (1991).
[25] J. Krok-Kowalski, H. Rej, T. Groń, J. Warczewski, T. Mydlarz,

and I. Okońska-Kozlowska, J. Magn. Magn. Mater. **137**, 329 (1995).
[26] U. von Barth and L. Hedin, J. Phys. C **5**, 1629 (1972).
[27] P. Hohenberg and W. Kohn, Phys. Rev. **136**, B864 (1964).
[28] W. Kohn and L. J. Sham, Phys. Rev. **140**, A1133 (1965).
[29] O. K. Andersen, Phys. Rev. B **12**, 3060 (1975).
[30] J. P. Perdew and Y. Wang, Phys. Rev. B **45**, 13244 (1992).
[31] P. E. Blöchl, O. Jepsen, and O. K. Andersen, Phys. Rev. B **49**, 16223 (1994).
[32] L. M. Sandratskii, J. Phys.: Condens. Matter **3**, 8565 (1991).
[33] D. M. Bylander and L. Kleinman, Phys. Rev. B **58**, 9207 (1998).
[34] V. I. Anisimov, J. Zaanen, and O. K. Andersen, Phys. Rev. B **44**, 943 (1991).
[35] A. I. Liechtenstein, V. I. Anisimov, and J. Zaanen, Phys. Rev. B **52**, R5467 (1995).
[36] A. N. Yaresko, V. N. Antonov, H. Eschrig, P. Thalmeier, and P. Fulde, Phys. Rev. B **62**, 15538 (2000).
[37] M. T. Czyżyk and G. A. Sawatzky, Phys. Rev. B **49**, 14211 (1994).
[38] I. A. Nekrasov, Z. V. Pchelkina, G. Keller, T. Pruschke, K. Held, A. Krimmel, D. Vollhardt, and V. I. Anisimov, Phys. Rev. B **67**, 085111 (2003).
[39] R. Arita, K. Held, A. V. Lukoyanov, and V. I. Anisimov, Phys. Rev. Lett. **98**, 166402 (2007).
[40] J. C. Slater and G. F. Koster, Phys. Rev. **94**, 1498 (1954).
[41] V. Eyert, K.-H. Höck, S. Horn, A. Loidl, and P. S. Riseborough, Europhys. Lett. **46**, 762 (1999).
[42] N. Shanthi, P. Mahadevan, and D. D. Sarma, J. Solid State Chem. **155**, 198 (2000).
[43] A. Continenza, T. de Pascole, F. Meloni, and M. Serra, Phys. Rev. B **49**, 2503 (1994).
[44] A. I. Liechtenstein, M. I. Katsnelson, V. P. Antropov, and V. A. Gubanov, J. Magn. Magn. Mater. **67**, 65 (1987).
[45] I. V. Solovyev and K. Terakura, Phys. Rev. B **58**, 15496 (1998).
[46] N. M. Rosengaard and B. Johansson, Phys. Rev. B **55**, 14975 (1997).
[47] A. Yaresko and V. Antonov, J. Magn. Magn. Mater. **310**, 1672 (2007).
[48] E. J. W. Verwey and E. L. Heilmann, J. Chem. Phys. **15**, 174 (1947).
[49] S. Pouget, M. Alba, N. Fanjat, and M. Nogues, Physica B **180**, 244 (1992).
[50] M. Schmidt, W. Ratcliff, P. G. Radaelli, K. Refson, N. M. Harrison, and S. W. Cheong, Phys. Rev. Lett. **92**, 056402 (2004).
[51] S.-H. Lee, D. Louca, H. Ueda, S. Park, T. J. Sato, M. Isobe, Y. Ueda, S. Rosenkranz, P. Zschack, J. Iniguez, Y. Qiu, and R. Osborn, Phys. Rev. Lett. **93**, 156407 (2004).
[52] N. Nishiguchi and M. Onoda, J. Phys.: Condens. Matter **14**, L551 (2002).